

© 2024 IEEE

Personal use of this material is permitted. Permission from IEEE must be obtained for all other uses, in any current or future media, including reprinting or republishing this material for advertising or promotional purposes, creating new collective works, for resale or redistribution to servers or lists, or reuse of any copyrighted component of this work in other works.

Cooperative Indoor Exploration Leveraging a Mixed-Size UAV Team with Heterogeneous Sensors

Michaela Cihlářová*, Václav Pritzl*^{ID}, Martin Saska*^{ID}

Abstract—Heterogeneous teams of Unmanned Aerial Vehicles (UAVs) can enhance the exploration capabilities of aerial robots by exploiting different strengths and abilities of varying UAVs. This paper presents a novel method for exploring unknown indoor spaces with a team of UAVs of different sizes and sensory equipment. We propose a frontier-based exploration with two task allocation strategies: a greedy strategy that assigns Points of Interest (POIs) based on Euclidean distance and UAV priority and an optimization strategy that solves a minimum-cost flow problem. The proposed method utilizes the SphereMap algorithm to assess the accessibility of the POIs and generate paths that account for obstacle distances, including collision avoidance maneuvers among UAVs. The proposed approach was validated through simulation testing and real-world experiments that evaluated the method’s performance on board the UAVs.

The paper is supported by the multimedia materials available at <https://mrs.felk.cvut.cz/case2024exploration>.

I. INTRODUCTION

Heterogeneous teams of UAVs with different roles, each equipped with different sensors, can handle diverse challenges by leveraging different capabilities. By combining Unmanned Aerial Vehicles (UAVs) with different sensory modes, endurance levels, and maneuvering skills, these teams can better adapt to complex and dynamic environments.

One such application is mapping indoor areas with narrow passages and openings. A team consisting of a bigger UAV with precise sensors and high computing capabilities and one or multiple smaller dependent UAVs capable of fitting through narrow entrances at the cost of sensor accuracy is especially suitable for such complex environments. The smaller UAVs can explore locations that are hard to reach, while the bigger UAV uses its onboard sensors to create global maps, synchronize the fleet, and guide the exploration. In addition to more reliable and precise localization of the entire team in the global map, this approach protects the more expensive UAV while the cheaper ones perform riskier tasks.

The incorporation of heterogeneity within UAV teams offers numerous benefits for exploratory missions. Yet, it also introduces several challenges that need to be addressed: how to allocate tasks among the UAVs according to their individual capabilities, how to coordinate the UAVs to achieve

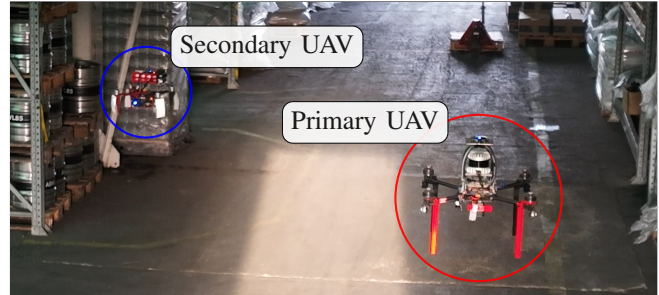


Fig. 1: UAV platforms used for experimental verification of the proposed method in real-world conditions: larger primary UAV, and smaller secondary UAV.

a common goal while respecting their constraints, and how to balance the trade-off between finding better solutions and ensuring real-time computation on board the UAVs. These challenges require careful attention to ensure that the benefits of heterogeneity outweigh the costs and do not compromise the overall effectiveness of the exploration mission.

In this paper, we propose an exploration strategy using a team of two closely cooperating UAVs; a larger, more-capable primary Unmanned Aerial Vehicle (pUAV), and a smaller, cheaper secondary Unmanned Aerial Vehicle (sUAV) (see Fig. 1). The intentional variation of UAV capabilities within the team enables it to quickly and accurately map spacious areas by the pUAV and simultaneously map confined spaces using the sUAV. This approach underscores the utility of heterogeneity in enhancing the efficiency and effectiveness of UAV-based exploration.

II. PROBLEM STATEMENT

We address the challenge of autonomous exploration of complex, Global Navigation Satellite System (GNSS)-denied environments through cooperative deployment of multiple UAVs featuring different physical characteristics and sensory capabilities. In this context, two UAVs are considered. The first is a larger pUAV, equipped with high computation power and a 3D Light Detection and Ranging (LiDAR) sensor with substantial range and high-precision data acquisition capabilities. The second is a comparatively smaller sUAV, intentionally designed to navigate through narrow spaces. However, it is limited to a Red-Green-Blue-Depth (RGBD) camera with considerably reduced Field of View (FOV) and lower-quality mapping functionality. The UAVs are capable of mutual communication over a wireless network, and the algorithms are designed to run fully on board the UAVs with no external computational resources utilized.

The task is to optimize the collaborative efforts of these

This work was funded by CTU grant no. SGS23/177/OHK3/3T/13, by the European Union under the project Robotics and Advanced Industrial Production (reg. no. CZ.02.01.01/00/22_008/0004590) and by the Czech Science Foundation (GAČR) under research project no. 23-07517S. *Authors are with the Department of Cybernetics, Faculty of Electrical Engineering, Czech Technical University in Prague, 166 36 Prague 6, {cihlamil|pritzlvac|martin.saska}@fel.cvut.cz

two UAVs to explore and map a priori-unknown environment where physical constraints and differing sensory inputs impact their exploration capabilities. This can be divided into the following components:

- 1) **Selecting Points of Interest (POIs)** - the challenge of selecting relevant points within the environment to guide the UAVs' exploration efforts.
- 2) **Accessibility Problem** - the consideration of accessibility constraints, particularly indoors with confined spaces, ensuring that the selected points are reachable by a specific UAV (pUAV or sUAV).
- 3) **Task Allocation** - the problem of distributing specific exploration tasks among the UAVs efficiently to maximize exploration coverage.
- 4) **Planning** - path planning strategies for the UAVs to navigate from their current location to the selected points of interest.
- 5) **Obstacle Avoidance** - the UAVs must safely navigate around static obstacles like walls and furniture, as well as dynamically moving objects (other UAVs).

In the method description, vectors are denoted with bold lowercase letters, matrices with bold uppercase italic letters, and frames of reference with uppercase upright letters. Sets and sequences are denoted by uppercase calligraphic letters. The transformation matrix describing the transition from frame A to frame B is represented as ${}^B_A\mathbf{T} \in SE(3)$. Let ${}^A\mathbf{x} \in \mathbb{R}^3$ be a 3D position vector in frame A, and let ${}^A\mathcal{P}_B$ be a sequence of UAV reference poses $({}^A\mathbf{x}_i, {}^A\phi_i)$, with position ${}^A\mathbf{x}_i \in \mathbb{R}^3$ and heading/yaw orientation ${}^A\phi_i \in [-\pi, \pi]$, for UAV B in reference frame A.

III. RELATED WORK

The exploration of unknown spaces has been addressed mainly through sampling-based and frontier-based approaches or their combinations. Sampling-based approaches, linked with the Next-Best-View (NBV) method [1]–[3], involve randomly sampling candidate viewpoints and selecting the one with the largest information gain. Frontier-based approaches [4]–[6] rely on identifying the frontiers, i.e., the boundaries between the known and unknown areas. Robots move toward these frontiers to gather information about the unexplored regions. In this work, a frontier-based approach is utilized as the accessibility of a specific frontier can be separately evaluated for each UAV and utilized for efficient goal assignment among the heterogeneous UAV team.

Our work focuses on creating a real-time system that is able to navigate safely through narrow passages, which requires fast and safety-aware planning. We obtain crucial information about the environment by using a volumetric occupancy grid such as the OctoMap [7]. However, long-distance planning on such a structure is time-consuming. In [8], the authors address this issue by creating a cache of the collision checking results. This reduced the planning time, but it would be inefficient for mixed-sized teams with different constraints. Another approach is to use a simplified, topological representation of the environment [9]–[11]. Some of these methods, however, do not focus on the safety of the

UAV [9] or are not suitable for large-scale exploration [10]. SphereMap approach [11] fills free space using intersecting spheres with a predefined minimal radius and creates a graph connecting the centers of the intersecting spheres. It is built continually on board a UAV during the mission, and stores precomputed paths for even faster planning. In our approach, SphereMap provides fast planning and computationally efficient checking of viewpoint reachability by differently-sized UAVs.

The research of multi-UAV teams and heterogeneous systems for exploration was supported by Defense Advanced Research Projects Agency (DARPA) Subterranean (SubT) Challenge [8], [12]–[15]. An approach using a topological representation of free space is proposed in [13]. It incorporates a team of one UAV and one Unmanned Ground Vehicle (UGV), but they explore the area separately, only occasionally sharing locally created maps. In [8], the authors focus on the effective use of both range and vision sensing modalities in multi-UAV teams. Nevertheless, the experiments were executed with a team consisting of multiple identical UAVs with the same set of sensors and also flying independently in their workspace.

In [16], the authors present a methodology for building inspection employing a team of UAVs. The approach utilizes LiDAR-equipped drones for initial exploration phases and camera-equipped drones for detailed inspection tasks. However, the research does not address variations in UAV sizes. Moreover, the UAVs equipped with cameras are restricted to navigating environments previously mapped by LiDAR drones.

Similarly, the advantages of a heterogeneous Nano Unmanned Aerial Vehicles (NAV) team with various equipment are studied in [17]. LiDAR-NAVs are tasked to perceive the surrounding environment, whereas an Edge-NAV collects data from LiDAR-NAVs and constructs the map. The study's focus is on creating a map representation based on OctoMap that is optimized for scenarios with limited memory capacity and offloading computational tasks to another NAV, but the experiments were again conducted with same-sized UAVs.

To achieve effective exploration, the operation area can be divided using Voronoi graph [18] or grid-based space decomposition [19]. However, such approaches are not desirable in the case of a mixed-size UAV team exploring a complex indoor space. Each area may contain spaces reachable by only the smaller UAV, along with large open areas that are quickly mappable by the larger UAV with better sensors. Therefore, the exploration method needs to distinguish between such spaces and assign them to the appropriate UAV with corresponding capabilities.

The contribution of this paper is summarized as a novel algorithm for frontier-based cooperative exploration of complex indoor spaces leveraging UAVs of different sizes and sensory equipment. The proposed approach was evaluated in realistic simulations and on board real UAV hardware with no external computational resources required, which proved its viability and real-time performance. To the best of our knowledge, no such cooperative exploration method

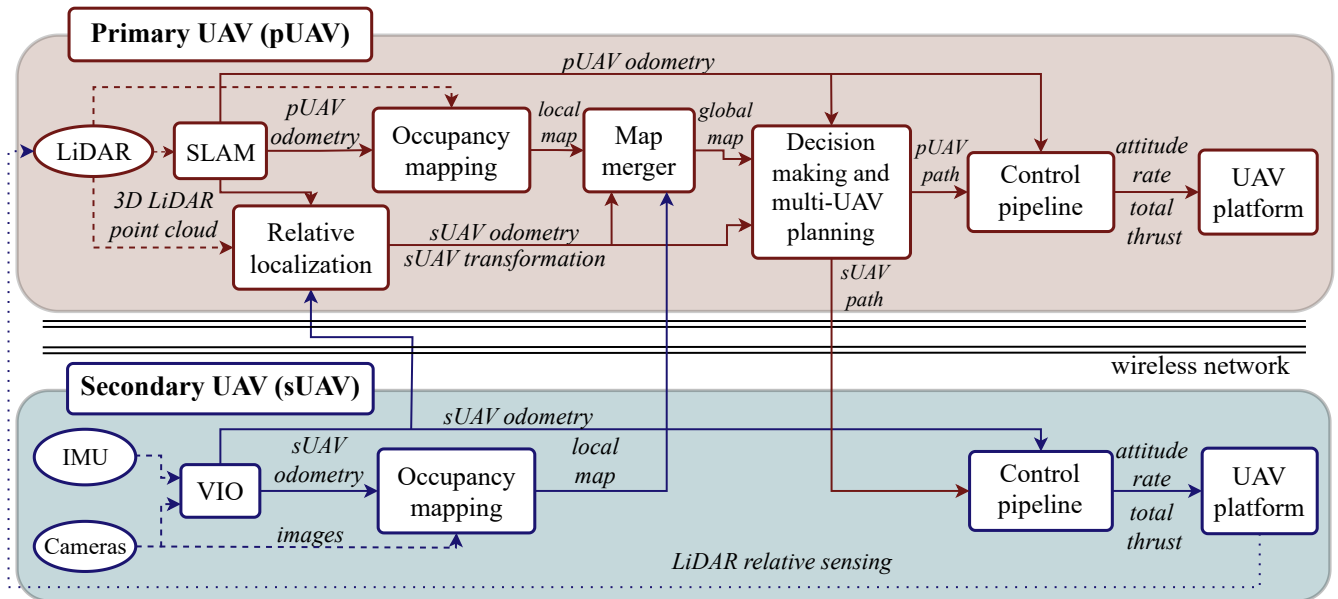


Fig. 2: Diagram of the multi-UAV software pipeline.

leveraging heterogeneity among mixed-sized UAVs has been proposed yet.

IV. MULTI-UAV EXPLORATION FRAMEWORK

The proposed approach is built on a software pipeline visualized in Fig. 2. The pUAV utilizes a 3D LiDAR Simultaneous Localization And Mapping (SLAM) algorithm for odometry computation and self-localization. The *Occupancy mapping* generates, using the OctoMap [7] approach, a local occupancy map ${}^P\mathcal{M}_P$ in pUAV's body frame P. *Relative localization* of the sUAV is achieved by identifying the sUAV within the LiDAR data and fusing the detections with sUAV Visual Inertial Odometry (VIO) odometry in sUAV's body frame S received over a wireless network. A detailed description of the relative localization method is in [20]. The *Map merger* algorithm creates a global occupancy map ${}^G\mathcal{M}$ in a common global frame G, facilitating high-level planning and decision-making.

The sUAV constructs a local occupancy map from the depth camera data and utilizes VIO for its self-localization. The sUAV VIO odometry and local occupancy map ${}^S\mathcal{M}_S$ are sent to the pUAV for collaborative control and planning.

The *Control pipeline* on board each UAV follows the desired UAV paths in the corresponding local reference using feedback control utilizing the corresponding self-localization data. Detailed information about the control pipeline is described in [21].

The novel *Decision-making and multi-UAV planning* algorithms are defined in the global frame G. Without loss of generality, we set the global frame G to be equivalent to the pUAV SLAM frame P for the specific case of a single LiDAR-equipped pUAV cooperating with a single camera-equipped sUAV. For better clarity, the superscript G, denoting the global frame, is omitted in the description of the algorithms unless its usage is necessary to prevent ambiguity.

The proposed exploration algorithm runs on board the pUAV without any external computational resources and coordinates the behavior of the entire UAV team. The algorithm consists of the following submodules, each running in parallel in a separate thread:

- 1) **Decision making** - A frontier detection algorithm identifies unexplored regions. The system assigns goals to individual UAVs, based on the goal's accessibility and distance, optimizing the distribution of exploration efforts across the fleet.
- 2) **Path planning** - The second thread handles the planning of paths to already selected POIs. It identifies UAVs completing their current task and requiring a new path. This ensures effective and continuous exploration of the unknown space.
- 3) **Collision avoidance** - The third thread addresses the crucial aspect of collision avoidance among UAVs. This algorithm continuously monitors the spatial dynamics of the two UAVs and employs safety measures if needed.

A. Selecting Points of Interest (POIs) and Accessibility

Frontiers are identified as unoccupied leaf nodes within the exploration area and next to unknown space. The algorithm clusters nearby frontiers based on Euclidean distance and selects the POIs from these clusters based on their centroids. In complex environments, additional random samples are drawn from each cluster for exploration. The frontier-based algorithm generates the set of POIs \mathcal{G} used by the Multi-Robot Task Allocation.

The key component of our work is ensuring the safety of drone operations. As mentioned in Sec. III, we propose an approach that utilizes the SphereMap.

An example of such a representation of free space can be seen in Fig. 3. SphereMap effectively reduces the computational complexity of path planning and obstacle avoidance.

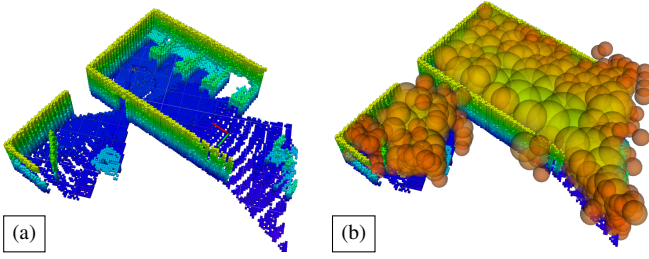


Fig. 3: Map representations using OctoMap (a) and SphereMap with OctoMap (b).

The SphereMap-based accessibility check is computationally efficient enough to operate in real time, even for a large number of POIs, thanks to precomputed paths. However, in practice, we aim to minimize the number of planned paths to reduce computational overhead. This is achieved by identifying the most interesting POIs by considering other criteria, as described in the following section.

B. Multi-Robot Task Allocation (MRTA)

The primary constraint in choosing algorithms for our mission is the necessity of real-time execution on board one of the UAVs in a dynamic environment. We compared two approaches: a simple greedy algorithm based on Euclidean distance and direction from the UAV and a more complex algorithm that formulates a Minimum-cost flow (MCF) problem.

We used the greedy approach to verify the functionality of the system and provide a baseline for comparison. To minimize the time required to change the heading of the sUAV, the greedy approach prefers points located in the same direction as the sUAV is facing. For pUAV, the heading change is not necessary, thanks to the 360° horizontal FOV of the 3D LiDAR. We propose to compute the costs c_{i_P} and c_{i_S} for each POI $g_i \in \mathcal{G}$ as

$$c_{i_P} = \|\mathbf{x}_P - \mathbf{g}_i\|_2 \quad (1)$$

$$c_{i_S} = \alpha \|\mathbf{x}_S - \mathbf{g}_i\|_2 + \beta |\phi_S - \theta_i|, \quad (2)$$

where $\alpha, \beta \in \mathbb{R}$ are predefined parameters.

The UAVs are assigned priority in goal selection to consider the different UAV sizes. The higher priority is assigned to pUAV as it fits only in spacious areas. The algorithm identifies the closest accessible point g_{P_n} for the pUAV by planning on SphereMap. Subsequently, it finds the first accessible point g_{S_n} for the sUAV using the same method, excluding the goal g_{P_n} chosen for the pUAV. If no accessible point is found, the UAV stays at its current position.

The advantages of such an approach include speed, low computational complexity, simplicity, and memory efficiency. However, its drawbacks lie in treating the UAVs independently rather than as a unified system. Furthermore, it does not consider path length, which can lead to high travel time despite proximity to the selected point.

To address these issues, we propose to represent the UAVs and the POIs as a bipartite graph $G = (U, V, E)$, where $\mathbf{x}_P, \mathbf{x}_S \in U$ are nodes represented by UAVs' position, $g_i \in V$ is a node which stands for corresponding POI i ,

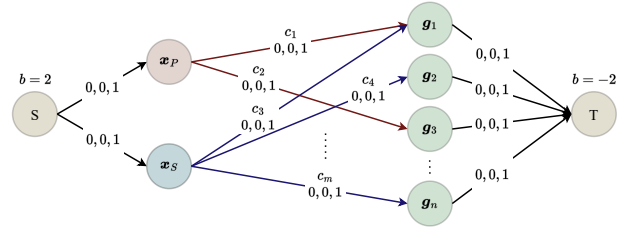


Fig. 4: Representation of the assignment problem as a minimum cost flow problem. The notation of edge labels 0, 0, 1 represent capacity's lower bound, current value, and upper bound u , respectively.

and $(\mathbf{x}, \mathbf{g}, c) \in E$ are edges defined by three values: starting node, end node, and cost c .

Thanks to the graph properties, we can formulate a flow problem. That requires a definition of the following terms:

- **Source Node** S is a single node that represents the start of the flow.
- **Sink Node** T is a single node representing the end of the flow.
- **Arcs** \mathcal{A} from a UAV to a POI exists if the UAV can safely visit the POI. The cost c of an arc is the weight of the corresponding edge in the bipartite graph.
- **Capacity** u of an arc from a UAV to a POI is one if the UAV can visit the POI. Otherwise, the capacity is 0 (in our case, these arcs are not created).
- **Balance** b refers to the conservation of flow at each node in the network. Each feasible solution must satisfy the fact that the amount of flow leaving minus the amount of flow entering the node must be equal to the node's balance.

Let \mathcal{N} be the set of all nodes, $f(a) \in \mathbb{R}_0^+$ the flow on arc $a \in \mathcal{A}$, $\delta^+(n)$ the set of arcs leaving node $n \in \mathcal{N}$, $\delta^-(n)$ the set of arcs entering node $n \in \mathcal{N}$, $c(a)$ the cost per unit of flow on arc $a \in \mathcal{A}$, $u(a)$ the capacity of arc $a \in \mathcal{A}$, and $b(n)$ the balance of node $n \in \mathcal{N}$. The MCF problem with zero lower capacity bound can be formulated as

$$\min_{a \in \mathcal{A}} c(a) \cdot f(a) \quad (3)$$

$$\text{s.t.} \quad \sum_{\forall a \in \delta^+(n)} f(a) - \sum_{\forall a \in \delta^-(n)} f(a) = b(n), \quad \forall n \in \mathcal{N}, \quad (4)$$

$$0 \leq f(a) \leq u(a), \quad \forall a \in \mathcal{A}. \quad (5)$$

The costs from the source node to each UAV x_i and from each POI g_i to the sink node are set to 0. These arcs exist only to transfer a matching problem to a flow problem and are irrelevant to the final solution. The balance for each node except source S and sink T is set to 0 (see Fig. 4 for an example).

Goal selection based on solving the MCF problem is described in Alg. 1. The algorithm creates priority queues, \mathcal{Q}_P and \mathcal{Q}_S , to manage the POIs' order based on the distance from the pUAV and the combined metric of distance and heading change from the sUAV. These computations are identical to Eq. 1 and 2. The assignment of the next goals involves iteratively selecting POIs g from these priority

queues, computing paths using SphereMap planning, and assessing the feasibility of the paths, given the UAV sizes s_P and s_S .

This algorithm proceeds to construct arcs, \mathcal{A}_P and \mathcal{A}_S , connecting the UAVs with accessible POIs, considering their associated costs and path length. Utilizing the priority queues \mathcal{Q}_P and \mathcal{Q}_S to examine the POIs in the specific order based on Eq. 1 and 2 minimizes the computational complexity. Parameter N is set, which indicates a sufficient number of arcs for each UAV, meaning that when there is already N accessible POIs found, no additional arcs for that UAV are created.

To ensure that the problem can be solved even if \mathcal{A}_P or \mathcal{A}_S is empty, special arcs $(\mathbf{x}_P, \mathbf{g}_{x_P}, c_{x_P})$ and $(\mathbf{x}_S, \mathbf{g}_{x_S}, c_{x_S})$, with high costs c_{x_P} and c_{x_S} , are created. Nodes \mathbf{g}_{x_P} and \mathbf{g}_{x_S} , added to the POIs' set, represent current \mathbf{x}_P and \mathbf{x}_S positions. So, if no accessible POIs are found, the UAV remains on its current position.

Then, the MCF problem is formulated. The nodes \mathcal{N} include: source S , sink T , the current positions of the UAVs \mathbf{x}_P and \mathbf{x}_S , the set of POIs \mathcal{G} , and the added points \mathbf{g}_{x_P} and \mathbf{g}_{x_S} . The set of all arcs \mathcal{A} contains arcs \mathcal{A}_{source} from source S to each UAV, arcs \mathcal{A}_{sink} from each POI $\mathbf{g}_i \in \mathcal{G}$ to sink T , and computed arcs \mathcal{A}_P and \mathcal{A}_S . The goals \mathbf{g}_{P_n} and \mathbf{g}_{S_n} are obtained by solving the MCF problem and selecting the POIs connected with each UAV position $\mathbf{x}_P, \mathbf{x}_S$ in the resulting graph with arc capacity 1.

C. Path Planning

The proposed path planning algorithm operates in two states: MONITORING and PLANNING. In the MONITORING state, the algorithm checks if either UAV $u \in \mathcal{U}$, where $\mathcal{U} = \{\text{pUAV}, \text{sUAV}\}$, has reached its current goal \mathbf{g}_{u_c} , creating a set of UAVs waiting for new path \mathcal{W} and updating the set of already visited points \mathcal{V} . When at least one UAV is waiting for a new action, the algorithm transitions to the PLANNING state.

The PLANNING stage is triggered by a map \mathcal{M} update to ensure that newly explored areas are also searched for POIs. Then, paths for each UAV $w \in \mathcal{W}$ are computed using the SphereMap. This approach is aligned with the priorities of fast computation and safety since the sUAV is designed to fly through narrow spaces. We did not use the precomputed paths during the planning process to obtain a smoother path.

The computed paths are transformed into the UAVs' local frames. For pUAV, the transformation matrix ${}^P_G\mathbf{T}$ is identity, and for sUAV, the matrix ${}^S_G\mathbf{T}$ is continuously updated by the relative localization.

Each UAV is then instructed to follow its respective path, and the algorithm returns to the MONITORING state.

D. Obstacle Avoidance

We assume that the environment does not contain dynamic obstacles, therefore only static obstacles and the possible collision of the two UAVs are considered. The static obstacles are handled by the planning process, and collision avoidance between UAVs is secured by creating three safety

Algorithm 1: Task allocation - assignment problem

Input: set of POIs \mathcal{G} , pUAV position \mathbf{x}_P , sUAV pose (\mathbf{x}_S, ϕ_S) , source node S , sink node T , arcs from source node \mathcal{A}_{source} , arcs to sink node \mathcal{A}_{sink}

Output: pUAV next goal \mathbf{g}_{P_n} , sUAV next goal \mathbf{g}_{S_n}

Parameters: pUAV size s_P , sUAV size s_S , cost c_{x_P} , cost c_{x_S} , number of maximum arcs N for each UAV

```

1  $\mathbf{g}_{x_P} \leftarrow \mathbf{x}_P, \mathbf{g}_{x_S} \leftarrow \mathbf{x}_S$ 
2  $\mathcal{Q}_P \leftarrow \text{PRIORITY\_QUEUE}(\mathcal{G}, \mathbf{x}_P) \triangleright$  based on distance from pUAV
3  $\mathcal{Q}_S \leftarrow \text{PRIORITY\_QUEUE}(\mathcal{G}, \mathbf{x}_S, \phi_S) \triangleright$  based on distance and heading change from sUAV
4  $\mathcal{A}_P \leftarrow \emptyset \triangleright$  arcs from pUAV
5  $i \leftarrow 0$ 
6 while  $i < N$  and  $\mathcal{Q}_P \neq \emptyset$  do
7    $c, \mathbf{g} \leftarrow \mathcal{Q}_P.\text{POP}() \triangleright$  cost and POI
8    $\mathcal{P} \leftarrow \text{FIND\_PATH}(\mathbf{x}_P, \mathbf{g}, s_P) \triangleright$  SphereMap
9   if  $\mathcal{P} \neq \emptyset$  then
10     $c \leftarrow c + \text{LENGTH}(\mathcal{P}) \triangleright$  number of waypoints
11     $\mathcal{A}_P \leftarrow \mathcal{A}_P \cup \{(\mathbf{x}_P, \mathbf{g}, c)\}$ 
12     $i \leftarrow i + 1$ 
13  end
14 end
15  $\mathcal{A}_P \leftarrow \mathcal{A}_P \cup \{(\mathbf{x}_P, \mathbf{g}_{x_P}, c_{x_P})\} \triangleright$  to secure feasibility
16 repeat lines 4-15 for sUAV with  $\mathcal{Q}_S, \mathbf{x}_S, s_S, \mathbf{g}_{x_S}, c_{x_S}$ , and  $\mathcal{A}_S$ 
17  $\mathcal{N} \leftarrow \{S, T, \mathbf{x}_P, \mathbf{x}_S\} \cup \mathcal{G} \cup \{\mathbf{g}_{x_P}, \mathbf{g}_{x_S}\}$ 
18  $\mathcal{A} \leftarrow \mathcal{A}_{source} \cup \mathcal{A}_{sink} \cup \mathcal{A}_P \cup \mathcal{A}_S$ 
19  $\mathbf{g}_{P_n}, \mathbf{g}_{S_n} \leftarrow \text{SOLVE\_MIN\_COST\_FLOW}(\mathcal{N}, \mathcal{A})$ 

```

zones based on the UAVs' distance. The first one, bounded by the critical distance d_C parameter, marks the area where the UAVs are too close to each other, and an avoidance maneuver is necessary. The maneuver takes advantage of the small size of the sUAV. The pUAV stops and is stationary the whole time. A new goal position \mathbf{g}_S is computed and assigned to the sUAV (the value of the z-axis stays the same as the current altitude):

$$\mathbf{u} = \frac{\mathbf{x}_S - \mathbf{x}_P}{\|\mathbf{x}_S - \mathbf{x}_P\|_2} \quad (6)$$

$$\mathbf{g}_S = \mathbf{x}_S + \mathbf{u} \quad (7)$$

$$\mathbf{g}_{S_z} = \mathbf{x}_{S_z} \quad (8)$$

$$\theta_S = \phi_S \quad (9)$$

The path \mathcal{P}_S to the goal \mathbf{g}_S is planned by an A*-based planner [22], on global map \mathcal{M} , ensuring that it is feasible, short, and safe. A path is found even if the goal \mathbf{g}_S is not accessible, but there is a reachable point in its proximity. This path is transformed to sUAV VIO frame S using transformation matrix ${}^S_G\mathbf{T}$ and sent to the control pipeline. When the sUAV reaches its goal, the whole process is repeated until the distance between the UAVs is bigger than the critical distance d_C .

In the second zone, when the distance is smaller than the safety distance d_S parameter but bigger than d_C , the safety of pUAV is prioritized, as it is equipped with more precise and more expensive sensors. The pUAV stops its action and waits until the sUAV, which continues in its current action, is far enough and the safety condition is satisfied:

$$\|\mathbf{x}_P - \mathbf{x}_S\|_2 \geq d_S \quad (10)$$

The last zone, where the distance is bigger than the safety distance d_S , is marked as safe, and the UAVs explore the space as described in previous sections.

V. EXPERIMENTAL VERIFICATION

We used two types of UAVs (see Fig. 1) that are controlled by the Pixhawk 4 Flight Controller with built-in Inertial Measurement Units (IMUs). The pUAV is based on the Holybro X500 frame and has a size of 0.7 by 0.7 meters, including propellers. It features a powerful onboard computer, the Intel NUC 10iFNH, with a Wi-Fi module for data transmission, and carries a 3D LiDAR Ouster OS0-128 Rev D, with a 360° horizontal and 90° vertical FOV, and range of 40 meters.

The sUAV, built around the DJI F330 frame with compact dimensions of approximately 0.45 by 0.45 meters, propellers included, is equipped with Intel NUC 10iFNH, the RealSense T265 tracking camera, and the RealSense D435 depth camera. The RealSense T265 incorporates two fisheye lens sensors with a 173° diagonal FOV, and an IMU. The RealSense D435 stereo-depth features infrared (IR) sensors with an 87° by 58° FOV and an Red-Green-Blue (RGB) sensor with a 69° by 42° FOV, alongside an IR projector with a range of 5 meters. For details of the platform setup, see [23].

The software is based on Ubuntu 20.04 and Robot Operating System (ROS) 1 Noetic, and the UAVs run on the Multi-robot Systems Group UAV system (MRS UAV system) [21], which allows for easy switching between simulation and real-world scenarios. Self-localization is achieved through SLAM algorithm LiDAR Odometry and Mapping (LOAM) [24], specifically Advanced implementation of LOAM (A-LOAM) for the pUAV, and the OpenVINS algorithm [25] offers a state-of-the-art, filter-based, VIO for the sUAV.

A. Simulations

The UAVs were tasked to explore an office environment of $23 \times 23 \times 3$ meters created in the Gazebo robotic simulator, visualized in Fig. 5. A spacious common area and multiple smaller rooms accessible through open doors, 0.9 meters wide, where only the sUAV can safely fit, were used to verify the cooperation between heterogeneous UAVs. Tab. I provides a list of parameters used for the simulations.

To evaluate the performance of the proposed algorithms in isolation from localization errors and to reduce the computational demands of the simulation, ground-truth data were used for self-localization of both UAVs and relative localization between the UAVs.

Fig. 6 shows the final occupancy map. It was obtained as the result of an exploration mission that lasted 4 minutes using the greedy approach to solve the task allocation

TABLE I: Parameters for the simulation experiments

Parameter	Notation	Value
OctoMap voxel size	\mathcal{M}_{res}	0.1 m
pUAV size (radius)	s_P	0.45 m
sUAV size (radius)	s_S	0.25 m
minimum safety distance	d_S	2.5 m
minimum critical distance	d_C	2.0 m
minimum radius of spheres	r_{sph}	0.35 m
frontier detection rate	F_{front}	0.5 Hz
path planning rate	F_{path}	2 Hz
collision avoidance rate	F_{coll}	10 Hz

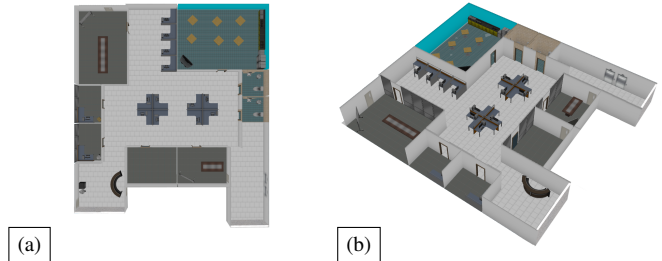


Fig. 5: Gazebo model of an office environment used for the experiments: top view (a), side view (b).

problem. The common, spacious area was explored by the pUAV, whereas the smaller rooms, accessible only through the doors, were explored only by the sUAV. For clarity, the floor and ceiling were removed from the visualization.

To analyze separate parts of the method, we measured the processing times of frontier detection, goal assignment, and path planning. These values were obtained during the experiments and provide a general idea about the algorithms' complexity. The results are shown in Fig. 7.

Frontier detection's processing time (see Fig. 7) depends on the map complexity. In an indoor environment, the processing time is significantly higher at the beginning of the exploration, as most of the leaf nodes to be explored are free. As the exploration progresses, the number of free leaf nodes $l \in \mathcal{M}_{free}$ is decreasing. The median processing time of frontier detection was 59.64 ms.

To compare the two algorithms for solving the task allocation problem, experiments with identical exploration parameters (see Table I) and identical UAVs' initial position were executed. The parameter N used in the MCF approach was set to $N = 5$, meaning the algorithm looks only for the first five accessible POIs for each UAV.

Both approaches successfully explored the environment and created the occupancy map visualized in Fig. 6. However, the MCF approach significantly improves the exploration efforts. As shown in Fig. 7, where the map exploration completion refers to the ratio of the explored volume of the map to the total volume of the map, it took 240.68 s to explore 95 % of the space using the greedy approach, whereas the MCF algorithm was able to achieve the same result in 186.55 s. The 95% boundary is marked by a red horizontal dashed line in Fig. 7, and the green vertical dashed lines correspond to t_{greedy} and t_{mcf} . If the greedy approach is considered the baseline solution, the MCF results in almost 30% improvement.

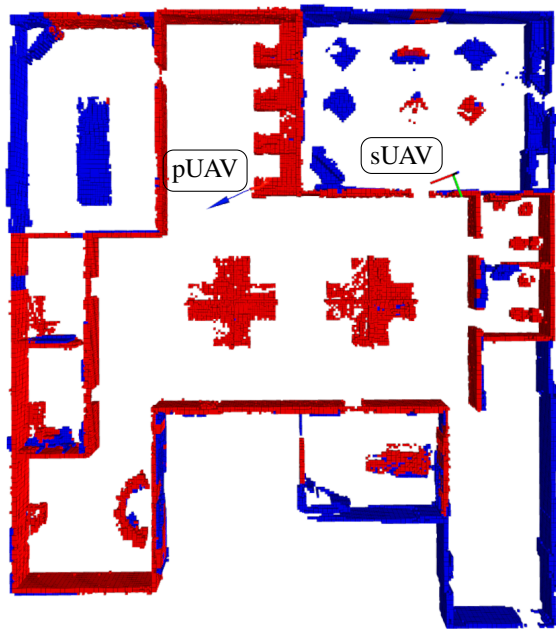


Fig. 6: Occupancy map of the office space at the end of the 4-minute mission. The red color represents an area scanned by the pUAV using LiDAR, and the blue color represents space explored only by sUAV.

However, the drawback of the MCF lies in higher execution time. The performance of the two algorithms was evaluated by measuring their respective processing times. The results are shown in Fig. 7 in a histogram of the goal assignment processing time of both algorithms created from 100 samples for each method. Even though the MCF approach overall speeds up the exploration, the computation of the global objective is more expensive. The median processing time of the greedy approach was 144.53 ms and the median processing time for the MCF approach was 253.76 ms.

The processing time of the path-planning algorithm differs based on the *state* variable. However, the processing time of the MONITORING state is insignificant in comparison to the PLANNING and, therefore, was not measured. The number of UAVs waiting for new action has the main effect on the time of the PLANNING state. Fig. 7 shows two peaks in the histogram, corresponding to the situation when either one or both UAVs need new paths.

B. Real-World Experiments

We tested the proposed algorithms in a real-world industrial warehouse environment (see Fig. 8) without any external localization system or computational resources. To ensure the safety of the UAVs, we updated the exploration parameters. The values are listed in Tab. II. The final map from one of the successful experiments is shown in Fig. 9. This map was obtained after a mission that lasted 4.1 minutes.

The experiments provided useful data regarding the real-life execution time of the proposed approach. The environment was complex, so random samples from the frontiers cluster were selected to enlarge the POIs's set.

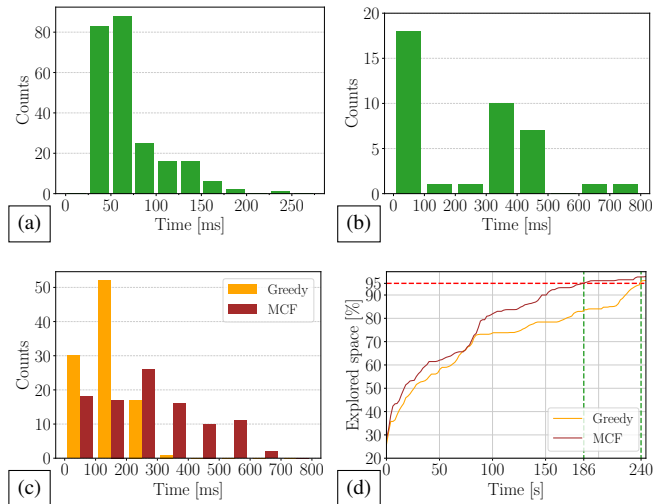


Fig. 7: Execution time of the algorithms in the office environment for frontier detection (a), path planning (b), goal assignment (c), and exploration time comparison (d).

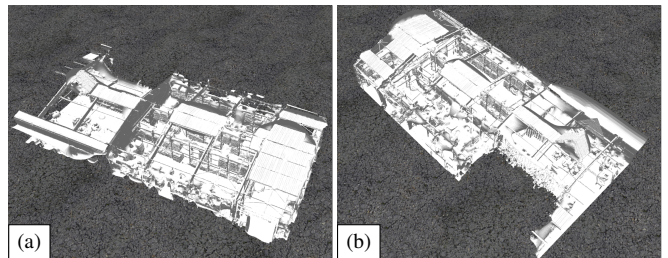


Fig. 8: 3D model of a warehouse environment where the real-world experiments were executed: front view (a), back view (b).

The assignment challenge was solved using the MCF, which outperformed the greedy method in simulation experiments. However, due to security measures, none of the POIs were reachable by the pUAV. This led to the worst-case scenario, where the accessibility of all the POIs had to be verified by computing and checking their paths at least once. Despite the large number of POIs, the maximum time required to solve the assignment problem was 1.15 s. This time was measured during the exploration, which confirms that the algorithm can handle large and complex environments. The median processing time for the frontier detection in this scenario was 178.2 ms, 842.12 ms for the assignment, and 23.49 ms for planning.

During the experiment, we noticed drifts in the estimated pose of the sUAV due to localization drift of the VIO

TABLE II: Parameters for real-world experiments

Parameter	Notation	Value
OctoMap voxel size	\mathcal{M}_{res}	0.1 m
pUAV size (radius)	s_P	1.8 m
sUAV size (radius)	s_S	0.4 m
minimum safety distance	d_S	4.0 m
minimum critical distance	d_C	3.5 m
minimum radius of spheres	r_{sph}	0.9 m
frontier detection rate	F_{front}	0.5 Hz
path planning rate	F_{path}	2 Hz
collision avoidance rate	F_{coll}	10 Hz

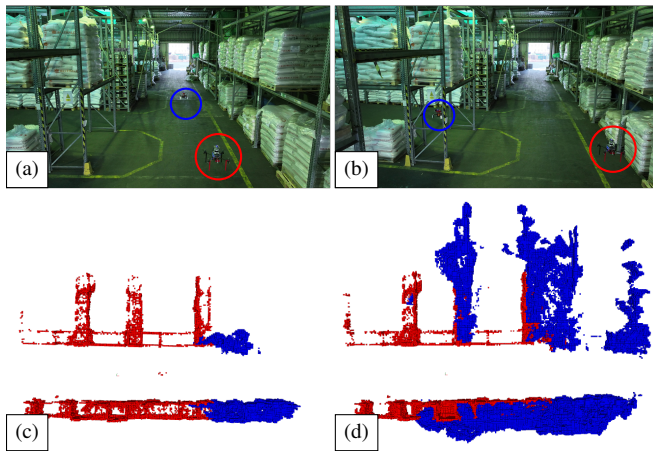


Fig. 9: Photographs from the real-world experiments (a), (b) and global occupancy grid at the initial position to show the exploration progress (c) and the final map (d).

when the line of sight between the UAVs was broken for a prolonged period of time. When the estimated pose was not correct, the path followed by the sUAV differed from the one planned on board the pUAV. This behavior is dangerous as it does not ensure the safety of the sUAV, and methods to select rendezvous points, where can pUAV correct this issues, are part of future work. Additionally, the large desired safety distances between the UAVs hindered the progress of the exploration, therefore, future work will focus on designing smaller UAVs with propeller protection.

The main purpose of the experiments was to prove that the proposed method is able to run in real time on the available hardware in real-world conditions with uncertainty. Even during the worst-case scenario, when there are no accessible POIs for pUAV, the algorithms are fast enough to ensure smooth exploration.

VI. CONCLUSION

We presented a novel method for unknown-space exploration using a heterogeneous team consisting of UAVs with different sizes and sensory equipment. The proposed approach utilizes a frontier-based method for generating Points of Interest, determining accessibility of the POIs using SphereMap, and solving the goal allocation problem using a minimum-cost flow technique. Collision-free paths to the selected POIs are generated and mutual distance between the UAVs is tracked to ensure safe flight. The algorithms were tested in a complex simulation environment, and their performance was evaluated in a real-world experiment on board the UAVs, which had no external localization system or external computational resources available. These experiments not only showed the properties of the proposed method but also provided valuable insights into its real-world applicability and potential for further improvement.

REFERENCES

[1] C. I. Connolly, "The determination of next best views," *IEEE ICRA*, vol. 2, pp. 432–435, 1985.
 [2] A. Bircher *et al.*, "Receding Horizon "Next-Best-View" Planner for 3D Exploration," in *IEEE ICRA*, 2016, pp. 1462–1468.

[3] L. Schmid *et al.*, "An Efficient Sampling-Based Method for Online Informative Path Planning in Unknown Environments," *IEEE Robotics and Automation Letters*, vol. 5, no. 2, pp. 1500–1507, 2020.
 [4] B. Yamauchi, "A frontier-based approach for autonomous exploration," *Proceedings IEEE International Symposium on Computational Intelligence in Robotics and Automation CIRA'97. 'Towards New Computational Principles for Robotics and Automation'*, pp. 146–151, 1997.
 [5] —, "Frontier-Based Exploration Using Multiple Robots," in *Proceedings of the Second International Conference on Autonomous Agents*, ser. AGENTS '98. New York, NY, USA: Association for Computing Machinery, 1998, p. 47–53.
 [6] B. Zhou *et al.*, "FUEL: Fast UAV Exploration Using Incremental Frontier Structure and Hierarchical Planning," *IEEE Robotics and Automation Letters*, vol. 6, no. 2, pp. 779–786, 2021.
 [7] A. Hornung *et al.*, "OctoMap: An efficient probabilistic 3D mapping framework based on octrees," *Autonomous Robots*, vol. 34, 2013.
 [8] G. Best *et al.*, "Resilient multi-sensor exploration of multifarious environments with a team of aerial robots," in *Robotics: Science and Systems (RSS)*, 2022.
 [9] T. Dang *et al.*, "Graph-based Path Planning for Autonomous Robotic Exploration in Subterranean Environments," in *IEEE/RSJ IROS*, 2019, pp. 3105–3112.
 [10] H. Cover *et al.*, "Sparse Tangential Network (SPARTAN): Motion planning for micro aerial vehicles," in *IEEE ICRA*, 2013, pp. 2820–2825.
 [11] T. Musil *et al.*, "SphereMap: Dynamic Multi-Layer Graph Structure for Rapid Safety-Aware UAV Planning," *IEEE Robotics and Automation Letters*, vol. 7, no. 4, pp. 11 007–11 014, 2022.
 [12] M. Petrlik *et al.*, "UAVs Beneath the Surface: Cooperative Autonomy for Subterranean Search and Rescue in DARPA SubT," *Field Robotics*, vol. 3, no. 1, p. 1–68, 2023.
 [13] M. Kulkarni *et al.*, "Autonomous teamed exploration of subterranean environments using legged and aerial robots," in *IEEE ICRA*, 2022, pp. 3306–3313.
 [14] N. e. a. Hudson, "Heterogeneous Ground and Air Platforms, Homogeneous Sensing: Team CSIRO Data61's Approach to the DARPA Subterranean Challenge," *Field Robotics*, vol. 2, no. 1, p. 595–636, 2022.
 [15] A. A. *et al.*, "NeBula: Quest for Robotic Autonomy in Challenging Environments; TEAM CoSTAR at the DARPA Subterranean Challenge," *arXiv pre-print*, 2021, arXiv: 2103.11470 [cs].
 [16] X. Xu *et al.*, "A Cost-Effective Cooperative Exploration and Inspection Strategy for Heterogeneous Aerial System," *arXiv pre-print*, 2024, arXiv: 2403.01225 [cs].
 [17] R. Xu *et al.*, "Cooperative and Autonomous Mapping for Heterogeneous NAVs," in *IEEE MASS*, 2023, pp. 539–547.
 [18] K. Masaba *et al.*, "GVGExp: Communication-Constrained Multi-Robot Exploration System based on Generalized Voronoi Graphs," in *International Symposium on Multi-Robot and Multi-Agent Systems (MRS)*, 2021, pp. 146–154.
 [19] B. Zhou *et al.*, "RACER: Rapid Collaborative Exploration With a Decentralized Multi-UAV System," *IEEE Transactions on Robotics*, vol. 39, no. 3, pp. 1816–1835, 2023.
 [20] V. Pritzl *et al.*, "Fusion of Visual-Inertial Odometry with LiDAR Relative Localization for Cooperative Guidance of a Micro-Scale Aerial Vehicle," *arXiv pre-print*, 2023, arXiv: 2306.17544 [cs].
 [21] T. Baca *et al.*, "The MRS UAV System: Pushing the Frontiers of Reproducible Research, Real-world Deployment, and Education with Autonomous Unmanned Aerial Vehicles," *Journal of Intelligent & Robotic Systems*, vol. 102, no. 1, 2021.
 [22] V. Krátký *et al.*, "An autonomous unmanned aerial vehicle system for fast exploration of large complex indoor environments," *Journal of Field Robotics*, vol. 38, no. 8, pp. 1036–1058, 2021.
 [23] D. Hert *et al.*, "MRS Drone: A Modular Platform for Real-World Deployment of Aerial Multi-Robot Systems," *Journal of Intelligent & Robotic Systems*, vol. 108, no. 4, 2023.
 [24] J. Zhang *et al.*, "LOAM : Lidar Odometry and Mapping in real-time," in *RSS*, 2014, pp. 109–111.
 [25] P. Geneva *et al.*, "OpenVINS: A Research Platform for Visual-Inertial Estimation," in *IEEE ICRA*, Paris, France, 2020.